

Classification of Visual Signs in Abdominal CT Image Figures in Biomedical Literature

Zhiyun Xue, Daekeun You, Sameer Antani, L. Rodney Long, Dina Demner-Fushman, George R. Thoma
National Library of Medicine, NIH, Bethesda, MD

ABSTRACT

“Imaging signs” are a critical part of radiology’s language. They not only are important for conveying diagnosis, but may also aid in indexing radiology literature and retrieving relevant cases and images. Here we report our work towards representing and categorizing imaging signs of abdominal abnormalities in figures in the radiology literature. Given a region-of-interest (ROI) from a figure, our goal was to assign a correct imaging sign label to that ROI from the following seven: accordion, comb, ring, sandwich, small bowel feces, target, or whirl. As training and test data, we created our own “gold standard” dataset of regions containing imaging signs. We computed 2997 feature attributes to represent imaging sign characteristics for each ROI in training and test sets. Following feature selection they were reduced to 70 attributes and were input to a Support Vector Machine classifier. We applied image-enhancement methods to compensate for variable quality of the images in radiology articles. In particular we developed a method for automatic detection and removal of pointers/markers (arrows, arrowheads, and asterisk symbols) on the images. These pointers/markers are valuable for approximately locating ROIs; however, they degrade the classification because they are often (partially) included in the training ROIs. On a test set of 283 ROIs, our method achieved an overall accuracy of 70% in labeling the seven signs, which we believe is a promising result for using imaging signs to search/retrieve radiology literature. This work is also potentially valuable for the creation of a visual ontology of biomedical imaging entities.

Keywords: image classification, abdominal CT imaging signs, content-based image retrieval, visual ontology

1. INTRODUCTION

Biomedical images are frequently used in the clinical and medical research literature to explain cases and demonstrate findings. These images provide useful information in addition to text that can be explored for enhancing publication retrieval. While some research works [1, 2] focus on analyzing the text in figure captions and the text in the article body that comments on the figure (“mentions”), a few studies [3, 4] investigate the use of content information extracted from images themselves. The latter is a new application of content-based image retrieval (CBIR). Our group has been conducting R&D in using both text and image information to search biomedical publications; we have also participated in the ImageCLEF medical retrieval track [5, 6]. This work has been incorporated into an online search engine called OpenI¹ (still under development) which currently provides access to over 600,000 figures from over 250,000 open access biomedical journal articles [7]. A screenshot of the system interface is shown in Figure 1.

In addition to this multi-modal retrieval, we are also conducting research to build a visual ontology for biomedical article retrieval [8], which is a relatively new research area. Similar to the ontologies used in the field of text, visual ontology aims to provide shared vocabulary by describing domain knowledge in terms of its concepts and relations. Specifically, it defines a set of visual entities and maps their appearances to text terms. A visual ontology can aid biomedical article retrieval in various aspects. For example, given a query image, the system can extract the text concepts that map the visual characteristics of the important regions in the query image, and then use the extracted text concepts to search the captions or mentions in the articles to retrieve related publications.

¹ <http://openi.nlm.nih.gov>



(a) Text query



(b) Image query

Figure 1. Screenshot of the OPENi system

The work presented in this paper is one building block that can be utilized for both multi-modal (visual + text) retrieval and visual ontology creation for biomedical information extraction. We focus on abdominal CT figures found in the radiology literature. Abdominal imaging remains one of the most complicated sub-specialties of diagnostic radiology. Computed tomography (CT) is one of the most important imaging techniques for visualizing and diagnosing abnormalities in the abdomen because of its relatively low cost and high image quality. CT imaging uses X-rays to generate images. Each pixel of the reconstructed image is assigned a number in Hounsfield units (HU) based on the cumulative amount of X-ray energy absorbed by tissue for that pixel location. In medical journals, CT images in figures are grayscale images converted from transforming the HU numbers (in the range of negative several thousands to positive several thousands) into pixel gray scale values [0, 255]. Major challenges we face for processing images obtained from biomedical publications include the large variations which occur with respect to image size, intensity illumination, viewing direction, anatomical position, pathology, and graphical annotations.

The present goal of our work is to associate a region-of-interest (ROI) in an abdominal CT image with a radiology concept associated with an abnormal finding. To do that, we construct a gold standard set of manually annotated ROIs. Specifically, we first identify typical imaging signs used by radiologists for recognizing abnormalities related with abdominal organs. Then, we collect image figures that have these imaging signs from online articles using several search engines and manually crop ROIs of each imaging sign with the guidance of captions and annotations on the images, such as arrows. Using a set of categorized ROIs, we train a supervised classifier which can then be used to label an input ROI with no associated text with a radiological imaging sign term. As the performance of the classifier relies significantly on the particular feature set used to represent the visual characteristics of ROIs, we first extract a generous number of color, texture, and shape descriptors and then employ a feature selection technique to reduce this large set of descriptors to a more tractable set of the “good” features, as determined by the selection technique. We also present a method for the automatic detection and removal of pointers/markers (arrows, arrowheads, and asterisk symbols) on the images. While these pointers are of great assistance in identifying the approximate locations of ROIs (which are important cues used for automatic ROI segmentation in our previous work [9]), they hamper the performance of classification because they are often (partially) included in the ROIs used to train the classifier. An image inpainting technique is applied to fill these pointer areas in order to alleviate this problem.

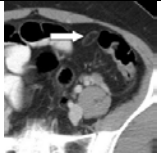
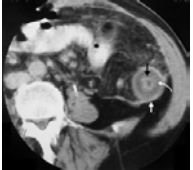
The rest of the paper is organized as follows. Section 2 describes the radiology imaging signs we used. Section 3 presents techniques about how the data is collected and processed, especially how the pointers (such as arrows) on the images are detected and removed. Section 4 explains the feature extraction, feature selection and the classifier we used. Section 5 presents classification performance and discussion. Section 6 concludes the paper and discusses future work.

2. IMAGING SIGNS

Abdominal CT interpretation is a demanding task because several organs, including liver, kidney, pancreas, spleen, stomach, colon, and small intestine can appear in the image. To successfully interpret abdominal CT, radiologists rely on understanding and recognizing *imaging signs* that are characteristic of complicated disease processes. Besides being important for diagnosis of abnormalities, imaging signs may also augment computer systems for indexing radiology

literature and retrieving relevant cases and images [10]. Many of these clinically important imaging signs are named with common objects that loosely resemble the corresponding imaging features. In this paper, we focus on the classic radiologic signs that are associated with intestines (colon and small intestine). Specifically, we identify seven classic imaging signs: *accordion* [11], *comb* [12], *ring* [13], *sandwich* [14], *small bowel feces (SBF)* [15], *target* [16], and *whirl* [17]. The characteristics of these signs and related conditions are listed in Table 1. A typical example of each imaging sign is also given in Table 1. The IDs of these imaging sign terms (except accordion sign) that are found in RadLex² are provided too.

Table 1. Imaging signs in abdominal CT

Imaging Signs	Characteristics and Conditions	Sample Images
Accordion sign	<ul style="list-style-type: none"> Described as alternating edematous haustral folds separated by mucosal ridges filled with oral contrast material, simulating appearance of an accordion Suggesting colonic edema or inflammation. 	 http://radiology.rsna.org/content/211/3/743.full
Comb sign RadLex ID: RID35101	<ul style="list-style-type: none"> Multiple tubular, parallel vessels that are visible on the mesenteric side of intestine, resembling comb teeth Indicating active Crohn's disease 	 http://radiology.rsna.org/content/230/3/783.full
Ring sign RadLex ID: RID35497	<ul style="list-style-type: none"> A thickened hyperattenuating rim around pericolonic lesion of higher attenuation than normal peritoneal fat Suggesting epiploic appendagitis 	 http://radiology.rsna.org/content/237/1/301.full
Sandwich sign RadLex ID: RID35514	<ul style="list-style-type: none"> The appearance of the homogeneous soft-tissue masses and the mesenteric fat and tubular structures in between resemble the two buns and the filling of a sandwich Indicating mesenteric lymphadenopathy 	 http://radiology.rsna.org/content/226/3/651.full
Small bowel feces sign RadLex ID: RID35552	<ul style="list-style-type: none"> The presence of heterogeneous matter intermingled with gas bubbles in the small intestine Suggesting small bowel obstruction 	 http://radiology.rsna.org/content/225/2/378.full
Target sign RadLex ID: RID35610	<ul style="list-style-type: none"> Thickened bowel wall having hyperattenuating inner and outer layers between which is a layer of low attenuation Nonspecific, but usually suggesting inflammatory process 	 http://radiology.rsna.org/content/234/2/549.full
Whirl sign RadLex ID: RID35699	<ul style="list-style-type: none"> Spinning pattern of superior mesenteric vein and midgut mesentery around superior mesenteric artery Indicating midgut volvulus 	 http://radiology.rsna.org/content/240/3/910.full

² <http://www.radlex.org/>

3. METHOD

Data Collection and Pre-processing

The data were collected online using search engines: ARRS GoldMiner, Google Image Search, National Library of Medicine’s OPENi, and Yale Image Finder. The downloaded images are accompanied with figure captions and discussion text from the article that describes it. The collected images have a large variety with respect to size and quality, suggesting the need for image resizing and contrast enhancement pre-processing steps. Also, many of the collected images contain pointers or text markers. These pointers (together with the texts) are important for identifying the locations of radiological signs when we create the labeled region-of-interest dataset. However, they also impede the subsequent steps of feature extraction and classification. Several examples are given in Figure 2. As shown in Figure 2, the pointers occupy a significant fraction of the ROIs (which are cropped from the original image). Since the features are calculated from the entire ROI, the existence of pointers interferes with the calculation of features for the ROI, and hence interferes with classification accuracy. To alleviate this hindrance, the pointers are extracted and the areas of pointers are filled using neighboring pixel intensities.

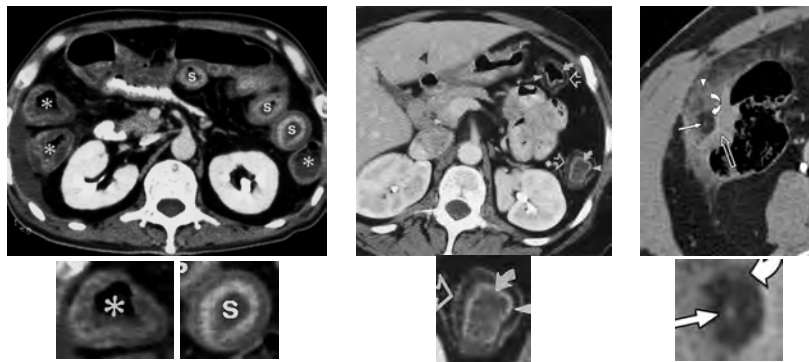


Figure 2. Pointers/markers interfere with feature extraction in the ROIs

3.1.1 Pointer Extraction

Pointer extraction is a difficult task due to two main challenges: (i) unconstrained pointing directions (rotation of pointers); and (ii) variety in pointer shapes. Figure 3 shows several pointer samples used in biomedical images, indicating that the pointer direction can be arbitrary and show large shape variations; note especially the tail shapes in the curved arrows.



Figure 3. Various shapes of pointers

To deal with this problem, we developed a pointer recognition algorithm based on Markov Random Fields (MRF) and Hidden Markov Models (HMM) [18]. Our algorithm consists of three steps as described below.

- 1) Pointer segmentation: This step detects pointer boundaries using edge detection and image binarization. Each pointer boundary is then approximated as a set of line segments.
- 2) MRF line segment labeling: Each line segment is labeled with a predefined line segment label by the MRF labeling method. We analyze a pointer as being a polygon made of seven line segments; these segments and their corresponding numeric labels are shown in Figure 4. The result of MRF labeling is a sequence of line segment labels (a “labeling configuration”) and is considered a robust representation of the pointer shape.

- 3) HMM pointer shape classification: Labeling configurations of pointers in the same class consist of nearly identical labels with similar sequence. This step classifies a pointer boundary into one of three pointer classes, viz., straight arrow (SA), curved arrow (CA), and arrowhead (AH). Our pointer recognition algorithm provides several important properties such as pointing direction, location of pointer tip, coordinates of boundary points, pointer color, and boundary length that can be used for additional information extraction (e.g., ROIs).

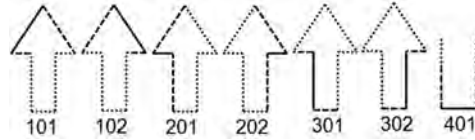


Figure 4. Sample line segment (solid line) and its label

In addition to the pointer recognition algorithm, we developed a neural network (NN) based algorithm to recognize asterisk symbols. We extracted several shape-based features and used them to train a NN classifier that classifies a boundary into one of two classes, viz., asterisk or non-asterisk.

3.1.2 Pointer Filling

To fill the pointer areas, we investigated two methods: mean color filling [19] and exemplar-based inpainting [20, 21]. For the mean color filling method, each pixel inside the pointer region is assigned the mean color of its non-zero neighbors in an iterative process starting from the boundary of the pointer region. The exemplar-based inpainting method has been proposed for replacing large objects in digital photographs. It uses an exemplar-based texture synthesis technique and a novel algorithm for determining the fill order of the holes. Figure 5 shows results of several region filling results obtained using these methods: mean color filled images tend to have blurs and lack texture, while the results of exemplar-based inpainting tend to have more visually plausible appearance. Compare Figures 5(b) and 5(c) to observe the capability of the exemplar-based inpainting method to propagate linear structures, such as lines and contours, across region holes; the region holes are dilated based on the ratio of pointer size to image size before the filling to ensure inclusion of entire pointer region.

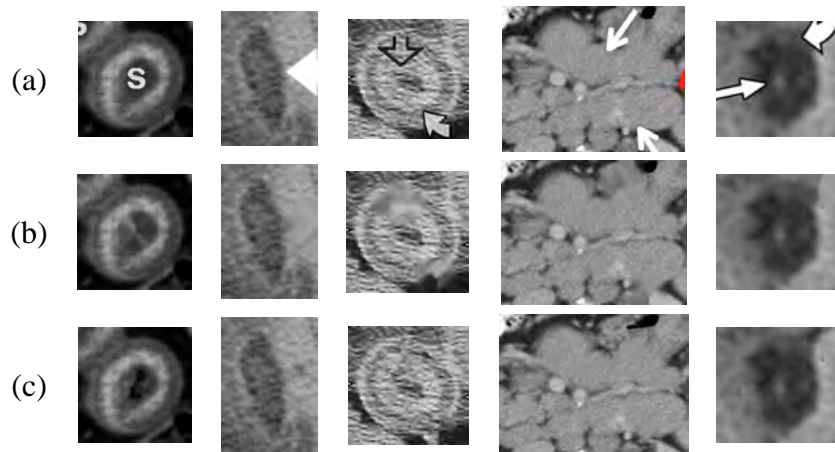


Figure 5. Pointer filling. (a) Original images; (b) Mean color filling; (c) Exemplar-based inpainting.

3.1.3 ROI Extraction

After the pointers are detected and filled, we manually cropped the regions-of-interest and labeled each ROI with one of the seven imaging signs. The labeling was done by computer scientists familiar with examples of these signs from the radiology literature. These manually labeled ROIs became our “gold standard” set of ROIs which we used to train a classifier. At the present state of our algorithm, given an input abdominal CT image, the user is required to manually specify an ROI, which is then classified with an imaging sign.

We have previously investigated the concept of automatic extraction of “ROI of interest” [18], where an automatic ROI extraction method was applied to thoracic CT images containing pointers/markers indicating an ROI. Briefly, after pointer detection, a square image region of a specified size (set as a system parameter) is cropped. If the pointer is a directional marker such as an arrow/arrowhead, the box is placed in the region where the pointer is pointing, and the tip of the pointer touches the center of one boundary of the box (illustrated in Figure 6a). If the pointer is a non-directional marker such as an asterisk symbol, the box is centered at the pointer (illustrated in Figure 6b). Clearly, the size of the ROI box is a critical parameter choice. In [18] for thoracic CT figures, we empirically determined a 200x200 pixel region as an appropriate size. Even though this automatic ROI extraction worked well for thoracic CT figures, it is not effective for abdominal CT data due to the following reasons:

- 1) The objects of imaging signs have significant variance in size even if the image size is the same. For example, the object with the sandwich sign (Figure 6(c1)) is much larger than that of the ring sign (Figure 6(c4)).
- 2) The directional pointers are not only used to point to an object of interest, but also point within the object (for example, a target sign which contains several layers (Figure 6(c2)) and an accordion sign which contains some branches (Figure 6(c3))). In addition, several pointers may be utilized to indicate one object.
- 3) In thoracic data, the visual characteristics of common abnormalities (such as “ground-glass opacity” or “mosaic attenuation patterns”) are texture patterns. Therefore, the size of the box is more elastic as long as the box is big enough to capture the texture pattern (which can be a fraction of the object region). This is in contrast to the abdominal data in which the size of the box is strict because it needs to capture the whole object (such as the ring sign (Figure 6(c4)) and target sign (Figure 6(c2))).

Notwithstanding the above challenges, the pointers provide significant information on the approximate location of the imaging sign. In our planned future work, we will investigate automatically cropping the ROI by utilizing *both* the pointers and the manually created gold standard set of ROIs.

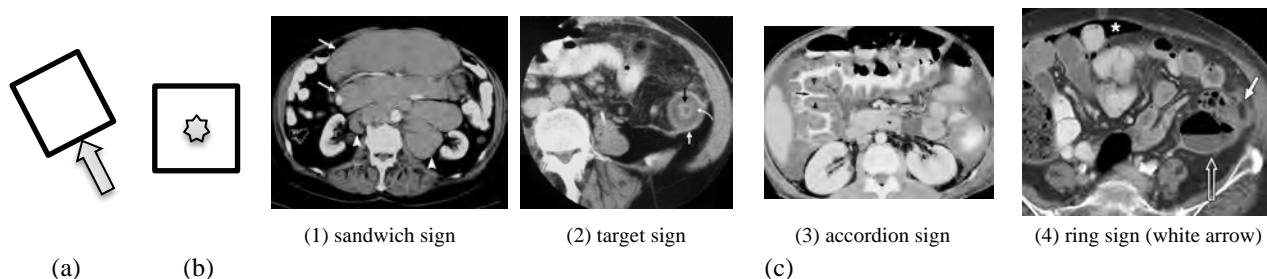


Figure 6. Challenges for automatic ROI extraction

Feature Extraction

To represent the visual information in ROIs, we calculated 18 feature descriptors. These features are used to characterize the color, texture, shape, edge, and spatial layout of pixels in the images. They include MPEG-7 features, Lucene image retrieval (LIRE) features, statistical texture features, scale-invariant feature transform (SIFT) features, local binary patterns (LBP), pyramid histogram of oriented gradients (PHOG), and Frangi filter-based features. All of the features and their corresponding dimensionalities are summarized in Table 2. After all features are extracted, each ROI is represented by a feature vector of length 2997.

Table 2. Features used to represent the visual characteristics of ROIs

Feature	Dimensionality
Color and edge directivity descriptor (CEDD) [22]	144
Fuzzy color and texture histogram (FCTH) [23]	192
Color layout descriptor (CLD) [24]	16
Edge histogram descriptor (EHD) [25]	80
Gabor filter descriptor [26]	60
Edge frequency	25
Tamura descriptor [26]	18

Color moments	3
Autocorrelation coefficients	25
Primitive length [27]	5
Gray-level co-occurrence matrix (GLCM) [27]	20
Scale Invariant Feature Transform (SIFT) [28]	256
Local binary patterns (LBP) [29]	256
Hu moments	5
Pyramid histogram of oriented gradients (PHOG) [30]	680
Hierarchical centroid [31]	124
Franqi filter based features [32, 33]	64
Local color histogram	1024
Combined feature	2997

Feature Selection and Classification

To reduce our extracted features to the most effective set, we used a supervised attribute selection method provided by WEKA [34]. This method requires the specification of (i) a feature evaluator which evaluates the utility (worth) of a subset of attributes by considering the individual predictive ability of each feature along with the degree of redundancy among the features; and (ii) a search method. For the latter we used the best-first algorithm, which searches the space of feature subsets by greedy hill-climbing augmented with a backtracking facility. We used a Support Vector Machine (SVM) for classification with a radial basis function as the kernel function for mapping the input feature vector into a high dimensional feature space. We used the Sequential Minimal Optimization (SMO) algorithm [35] implemented in WEKA for training the SVM multi-class classifier.

4. EXPERIMENTAL RESULTS AND DISCUSSION

Using the imaging sign terms defined in RadLex and radiology journal articles, we collected a total of 335 abdominal CT scans and their associated captions/texts from the Web. We pre-processed the images, extracted/filled the pointer areas, and manually cropped the ROIs containing the imaging signs. Then we extracted features from the ROIs, applied feature selection, and trained and tested an SVM classifier.

Pointer extraction

Table 3 shows our pointer extraction result. Out of a data set with 705 pointers, our algorithm detected 569 pointers, of which 511 were true positives. Our method achieved 89.8% and 72.5% precision and recall, respectively. The failures were due to: i) failure in pointer segmentation, and ii) failure in pointer recognition. Segmentation failure was mainly responsible for missing (undetected) pointers. Low image quality (e.g., low resolution or low contrast pointer boundary) was a major factor that adversely affected the results. In low resolution images, even correctly segmented pointers may be considered as noise and removed because their sizes are smaller than the threshold.

Table 3. Pointer extraction result

	Ground truth	Detected	Detected true	Precision (%)	Recall (%)
# of pointers	705	569	511	89.8	72.5

ROI manual extraction

After applying the exemplar-based inpainting method to fill the areas of the correctly recognized pointers in the images, we manually cropped and obtained a total of 283 ROIs relating to 7 imaging sign terms (accordion: 33, comb: 37, ring: 60, sandwich: 18, SBF: 38, target: 31, and whirl: 66). These ROIs are then used for multi-class classifier training and testing.

Table 4. Collected ROIs

	Accordion	Comb	Ring	Sandwich	SBF	Target	Whirl
# of ROIs	33	37	60	18	38	31	66

Feature selection and classification

We split the data into two sets. We used 2/3 of the data as a training set for feature selection and classifier training. The rest of the images were used for classifier testing. Using the training set, 70 out of 2997 feature attributes were selected. The classification performance (evaluated using TP rate, FP rate, precision, recall, F-measure, ROC area) for the testing set (using the 70 selected features) is given in Table 5 (a). To demonstrate the value of the step of pointer filling, we also evaluated the performance of our ROI classifier on the dataset in which the pointers are not filled. The results are given in Table 5(b). The overall classification accuracies for the dataset with pointer filling and the dataset without pointer filling are 70.2% vs. 64.9%. These numbers demonstrate the effectiveness/necessity of pointer recognition and filling.

Table 5. Classification results of testing set

	(a) with pointers filled						(b) without pointers filled					
	TP Rate	FP Rate	Precision	Recall	F-Measure	ROC Area	TP Rate	FP Rate	Precision	Recall	F-Measure	ROC Area
accordion	1	0.036	0.786	1	0.88	0.988	0.909	0	1	0.909	0.952	0.993
comb	0.5	0.061	0.545	0.5	0.522	0.805	0.5	0.085	0.462	0.5	0.48	0.877
ring	0.65	0.054	0.765	0.65	0.703	0.88	0.55	0.081	0.647	0.55	0.595	0.88
sandwich	0.833	0	1	0.833	0.909	0.999	0.667	0	1	0.667	0.8	0.987
Small bowel feces	0.692	0.049	0.692	0.692	0.692	0.945	0.462	0.062	0.545	0.462	0.5	0.876
target	0.7	0.048	0.636	0.7	0.667	0.923	0.5	0.012	0.833	0.5	0.625	0.896
whirl	0.803	0.060	0.803	0.803	0.667	0.856	0.864	0.194	0.576	0.864	0.648	0.848
Overall accuracy	70.2%						64.9%					

5. CONCLUSIONS

Searching/Retrieving images within peer-viewed biomedical literature has become an active research topic due to the prevalence of these images and the rich information they can provide for researchers and clinicians. In this paper, we present our initial efforts towards retrieving abdominal CT images in radiology articles. Specifically, we develop a classification method that labels image regions based on imaging signs. Imaging signs are characteristic imaging features of anomalies that are often seen in radiologic practice and are used by radiologists to recognize abnormalities and diagnose disease. Therefore they are of great significance for radiology study and relevant case retrieval. One identifiable challenge we face in this work is the intrinsic large variability presented among article figures with respect to image content, quality, and size. The feasibility of the proposed approach is demonstrated by the experimental tests and the results are encouraging. We also present a method to automatically recognize and replace the pointers (arrows and symbols) that are often contained in biomedical articles. Future work includes the expansion of the dataset, the addition of additional shape features, and the development of automatic extraction of region-of-interest for figures containing arrows.

ACKNOWLEDGEMENT

This research was supported by the Intramural Research Program of the National Institutes of Health (NIH), National Library of Medicine (NLM), and Lister Hill National Center for Biomedical Communications (LHNCBC).

REFERENCES

1. H. Yu and M. Lee M, "Accessing bioscience images from abstract sentences", *Bioinformatics*, 22(14): e547-e556, 2006.
2. M. A. Hearst, A. Divoli, H. Guturu, A. Ksikes, P. Nakov, M. A. Wooldridge, and J. Ye, "BioText search engine: beyond abstract search", *Bioinformatics*, 23: 2196-2197, 2007.
3. S. Xu, J. McCusker, M. Krauthammer, "Yale Image Finder (YIF): a new search engine for retrieving biomedical images," *Bioinformatics*, 24(17):1968-1970, 2008.
4. H. Müller, P. Clough, T. Deselaers, and B. Caputo, "Experimental evaluation in visual information retrieval", *The Information Retrieval Series 32*, Springer, 2010.

5. M. Simpson, M. M. Rahman, S. Phadnis, E. Apostolova, D. Demner-Fushman, S. K. Antani, and G. R. Thoma, "Text- and content-based approaches to image modality classification and retrieval for the ImageCLEF 2011 medical retrieval track", CLEF 2011 Working Notes. Amsterdam, Netherlands. September 2011.
6. M.M. Rahman, S. K. Antani, G. R. Thoma, "A learning-based similarity fusion and filtering approach for biomedical image retrieval using SVM classification and relevance feedback", *IEEE Transactions on Information Technology in Biomedicine*,15(4):640-646, July 2011.
7. D. Demner-Fushman, S. K. Antani, G. R. Thoma, "Multimodal biomedical information retrieval", The Fourth International Symposium on Languages in Biology and Medicine (LBM 2011), Nanyang Technological University, Singapore, December 2011.
8. M. Simpson, D. You, M. M. Rahman, S. K. Antani, G. R. Thoma, D. Demner-Fushman, "Towards the creation of a visual ontology of biomedical imaging entities", *AMIA Annual Symposium Proceedings*, 866-875, 2012.
9. D. You, S. Antani, D. Demner-Fushman, M. Rahman, V. Govindaraju, and G. R. Thoma, "Automatic identification of ROI in figure images toward improving hybrid (text and image) biomedical document retrieval", *Proceedings of SPIE Electronic Imaging Science and Technology, Document Retrieval and Recognition XVIII*, San Francisco, CA, 7874:78740K, January 2011.
10. M. W. Shore, D. L. Rubin, C. E. Kahn Jr., "Integration of imaging signs into RadLex", *Journal of Digital Imaging*, 25(1): 50-55, February 2012.
11. M. Macari, E. J. Balthazar, A. J. Megibow, "The accordion sign at CT: a nonspecific finding in patients with colonic edema", *Radiology*, 211:743-746, 1999.
12. A. J. Madureira, "The comb sign", *Radiology*, 230(3):783-784, 2004.
13. A. Rajesh, "The ring sign", *Radiology*, 237(1):301-2, 2005.
14. S. M. Hardy, "The sandwich sign", *Radiology*, 226(3):651-652, 2003.
15. M. H. Fuchsjäger, "The small-bowel feces sign", *Radiology*, 225(2):378-379, 2002.
16. J. Ahualli, "The target sign: bowel wall", *Radiology*, 234(2):549-550, 2005.
17. M. Epelman, "The whirlpool sign", *Radiology*, 240(3):910-911, 2006.
18. D. You, S. Antani, D. Demner-Fushman, M. M. Rahman, V. Govindaraju, G. R. Thoma, "Biomedical article retrieval using multimodal features and image annotations in region-based CBIR", *Document Recognition and Retrieval XVII* 7534(1), 75340V+, SPIE, San Jose, California, USA, 2010.
19. G. Zimmerman and H. Greenspan, "Automatic detection of specular reflections in uterine cervix images", *Proc. of SPIE Medical Imaging*, 6144:2037-2045, 2006
20. A. Criminisi, P. Perez, K. Toyama, "Region filling and object removal by exemplar-based image inpainting", *IEEE Transactions on Image Processing*, 13(9):1200-1212, 2004.
21. <http://www.cc.gatech.edu/~sooraj/inpainting/>
22. S.A. Chatzichristofis, Y.S. Boutalis, "CEDD: Color and edge directivity descriptor: A compact descriptor for image indexing and retrieval", In: Gasteratos, A., Vincze, M., Tsotsos, J.K. (eds.) *Proceedings of the 6th International Conference on Computer Vision Systems. Lecture Notes in Computer Science*, 5008:312-322, Springer- Verlag Berlin Heidelberg, 2008.
23. S.A. Chatzichristofis, Y.S. Boutalis, "FCTH: Fuzzy color and texture histogram: A low level feature for accurate image retrieval", In: *Proceedings of the 9th International Workshop on Image Analysis for Multimedia Interactive Services*, 191-196, 2008.
24. S. F. Chang, T. Sikora, A. Puri, "Overview of the MPEG-7 standard", *IEEE Transactions on Circuits and Systems for Video Technology*, 11(6): 688-695, 2001.
25. M. Lux, "Caliph & Emir: MPEG-7 photo annotation and retrieval", *Proceedings of the seventeen ACM international conference on Multimedia*, pp. 925-926, 2009, Beijing, China.
26. P. Howarth and S. Ruger, "Robust texture features for still image retrieval", *IEEE Proceedings of Vision, Image & Signal Processing*, 152(6): 868-874, December 2005.
27. G.N. Srinivasan, G. Shobha, "Statistical texture analysis", *Proc. World Acad. Sci. Eng. Technol.*, 36:1264-1269, 2008.
28. D.G. Lowe, "Distinctive image features from scale-invariant keypoints", *International Journal of Computer Vision*, 60 (2): 91-110, 2004.

29. G. Zhao, M. Pietikäinen, “Dynamic texture recognition using local binary patterns with an application to facial expressions”, *IEEE Trans. Pattern Analysis and Machine Intelligence*, 29(6):915-928, 2007.
30. A. Bosch, A. Zisserman, X. Muñoz, “Representing shape with a spatial pyramid kernel”, *International Conference on Image and Video Retrieval*, Amsterdam, The Netherlands, July 2007.
31. A. Shahar, “Handwriting recognition and fast retrieval for Hebrew historical manuscripts”, *Master’s Thesis*, The Hebrew University of Jerusalem, December 2011.
32. S. Jaeger, C. Casas-Delucchi, M. Cardoso, and K. Palaniappan, “Classification of cell cycle phases in 3D confocal microscopy using PCNA and chromocenter features,” in *7th Indian Conference on Computer Vision, Graphics, and Image Processing*, Chennai (India), pp. 412–418, 2010.
33. A. Frangi, W. Niessen, K. Vincken, and M. Viergever, “Multiscale vessel enhancement filtering,” in *Medical Image Computing and Computer-Assisted Intervention (MICCAI)*, pp. 130–137, 1998.
34. M. Hall, E. Frank, G. Holmes, B. Pfahringer, P. Reutemann, I. H. Witten, “The WEKA data mining software: an update”, *SIGKDD Explorations*, 11(1):10-18, November 2009.
35. J. Platt, “Sequential minimal optimization: a fast Algorithm for training support vector machines”, *Technical Report MSR-TR-98-14*, Microsoft Research, 1998.